Beyond the random-phase approximation in nonlocal-density-functional theory

C. D. Hu* and David C. Langreth
Serin Physics Laboratory, Rutgers University, Piscataway, New Jersey 08854
(Received 24 April 1985)

The previous work by Langreth and Perdew and by Langreth and Mehl for calculation of the exchange-correlation density functional is put on the same sort of basis as standard calculations for the uniform system by the approximate calculation of the following terms which go beyond the random-phase approximation (RPA): the second-order exchange term and self-energy corrections of similar order. It is found when *both* local [local-density approximation (LDA)] *and* nonlocal terms are included, that the net effect of these additional terms is found to be small, so that the RPA previously used is a much better approximation than previously supposed. Evidence is presented that suggests for localized systems that the leading non-RPA terms in the LDA represent mostly a spurious self-interaction error which is removed when the nonlocal beyond-RPA terms are included as well; it is suggested that this error can be most simply avoided by just using the RPA alone for both the local and nonlocal contributions, as done in the simple approximation suggested by Langreth and Mehl [Phys. Rev. B **28**, 1809 (1983)].

I. INTRODUCTION

The Kohn-Sham method[1] is now widely used for the calculation of the ground-state properties of solids, surfaces, and molecules. An input to such calculations is an approximation to the exchange-correlation energy as a functional of the density. The uncertainties are of two types: (1) what is the best correlation energy for a uniform system [i.e., what is the best form for the local-density approximation (LDA)], and (2) what are the nonlocal corrections?

Vosko *et al.*[2] have recently done a thorough critical study of the various calculations available for the uniform system. By the criteria set there certain classic approximate methods such as the Wigner interpolation formula[3] and the random-phase approximation[4] (RPA) are eliminated as viable contenders for providing the best available expressions for the correlation energy of a uniform system as a function of density. Vosko *et al.*[2] also explicitly eliminated some of the more recent calculations. We believe that this analysis is generally correct, although later in the present paper we will present an unexpected twist to the argument.

von Barth[5] has just reviewed the various schemes to go beyond the LDA. The present paper deals with the method recently espoused by our own group.[6–8] This scheme of Langreth and Mehl[6,7] (LM) used the RPA as the basic diagrammatic approximation method: RPA calculations for the nonlocal terms had been carried out previously;[9] these were adapted and used by LM. They argued, in addition, that because of the known cancellation between local and nonlocal effects, it would be inconsistent to use any approximation but the RPA for the local part. It would seem desirable to consider the effect of going beyond the RPA in both LDA and beyond-LDA terms. This is the principal aim of this paper.

Another concern is the relationship between the beyond-LDA corrections derived in LM (and in the present paper) and the fact that the LDA spuriously counts the interaction (electrostatic, exchange, and correlation) between an electron and itself. Perdew and Zunger[10] have made a systematic study of this self-interaction error and have espoused an approximate scheme for correcting it; this scheme was used to predict corrections to the LDA which at least for atomic inner shells were of a magnitude similar to the LM correction. In addition, Norman and Koelling[11] have used the method to produce exchange-correlation potentials whose nonlocal correction is very similar to those calculated by the LM method, which in turn were very similar to the exact potentials of Talman *et al.*[12] Of course, in an exact density-functional theory there would be no self-interaction error. Since the LM correction as well as those proposed here purport to make the LDA more exact, they should contain terms which mimic self-interaction corrections. Later in the paper we identify one such term. In fact, we will present evidence that in at least one fairly common situation the difference between the RPA (in the LDA) and a "better"[2] LDA energy expression is almost entirely a self-interaction error which is canceled when beyond-LDA terms are included. This result agrees with the observation of Cole and Perdew[13] that, in the Perdew-Zunger scheme, it makes little numerical difference whether beyond-RPA terms are included or not, although in the LDA it can make a substantial difference.

There are two by-products of this work which may have some use in their own right. The first is a new calculation of the electron-gas correlation energy as a function of the interparticle distance r_s. Although this may not be quite "state of the art" in accuracy, it is much better than the RPA, it satisfies the criteria of Vosko *et al.* for a viable approximation, and, in fact, it is numerically almost identical to the calculation of Singwi *et al.*[14] (SSTL); this latter calculation is the one parametrized by Hedin and Lundqvist[15] and widely used in electronic-structure calculations. The advantage of our calculation is that it is feasible to generalize to nonuniform situations.

This calculation is described in Sec. II.

The second by-product of this work is just such a generalization. In Sec. III the method of approximation of Sec. II is applied to calculate the beyond-RPA correction to the gradient expansion.[9,16,17] The results are collected in Sec. IV. Finally, in Sec. V we get to our original aim of presenting evidence that the beyond-RPA local terms are mostly a self-interaction error canceled by beyond-RPA nonlocal terms. We conclude that the Langreth-Mehl[6,7] nonlocal correction coupled with the RPA local terms (e.g., von Barth–Hedin) still represents the best approximation that has come from this type of analysis.

II. THE CORRELATION ENERGY OF THE UNIFORM GAS—A SIMPLE ADEQUATE APPROXIMATION

In this section we calculate the correlation energy of a uniform electron gas. Three criteria were used for selecting a method: (i) it must be simple; (ii) it must be expressible at least approximately in terms of "Φ-derivable"[18] set of diagrams; (iii) it must represent a substantial improvement over the RPA and preferably be comparable to state of the art calculations. Requirements (i) and (ii) are necessary to make a generalization to nonuniform systems reasonably possible and consistent, while (iii) is necessary for our results to be meaningful.

We begin with a brief summary of what is known about the correlation energy (per electron) E_c as a function of r_s [as usual, $r_s=(3/4\pi n)^{1/3}$, and we pick units so that lengths are in bohrs and energies in rydbergs]. For reference the value of $E_c(r_s)$ within the RPA (Ref. 4) is shown in Fig. 1. For high density ($r_s \ll 1$) it takes the form[19]

$$E_c^{\mathrm{RPA}}=0.0622\ln r_s-0.142\ \mathrm{Ry}\ . \tag{2.1}$$

We now follow Vosko *et al.*[2] and discuss the difference $\Delta E_c=E_c-E_c^{\mathrm{RPA}}$. Figure 2 includes (along with other information) what is known about this quantity. The solid dot at $r_s=0$ is known exactly.[19,20] The open circles represent Ceperly's and Alder's[21] exact stochastic sampling of the solution of Schrödinger's equation for samples with $\sim 10^2$ particles. Their error bars, which include statistical error, are invisible on this scale; however, the errors involved in extrapolating to the thermodynamic limit are hard to estimate and may well be larger. The squares represent the Vosko-Wilk-Nusair[2] average of modern calculations deemed includable. The bars associated with these points are not error bars, but rather the standard deviations of the calculations included in the average. We will use the above-mentioned points to assess the approximation scheme to be described below.

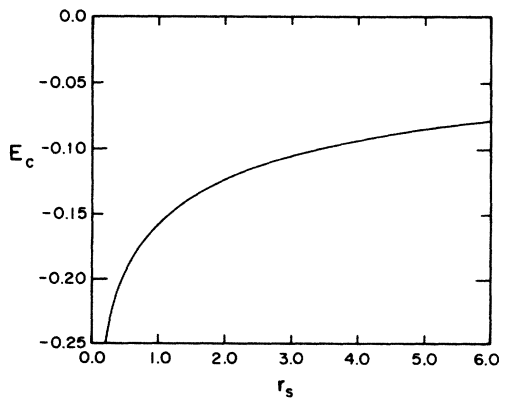

FIG. 1. Correlation energy of a uniform electron gas (in Ry) calculated with the RPA, versus r_s, the radius of the Wigner-Seitz sphere.

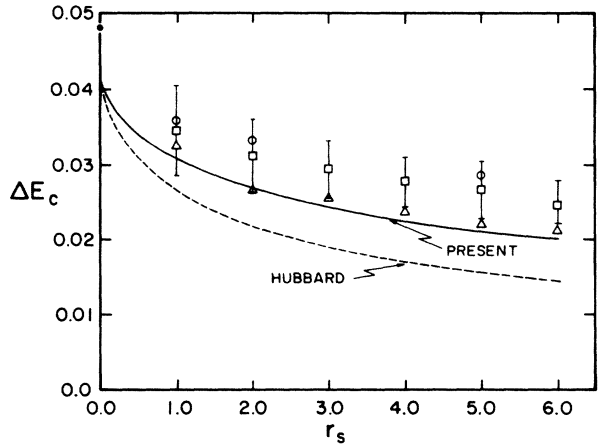

FIG. 2. ΔE_c, the correction to RPA correlation energy, versus r_s for the uniform electron gas. We show our result (solid curve) along with those of Hubbard's approximation (dashed curve), SSTL (triangles), the Ceperley-Alder simulation (open circles), and the average of Vosko *et al.* (squares). The solid dot at $r_s=0$ is the one known exact point. See text for the meaning of the bars.

In Fig. 3 we illustrate the diagrammatic expansion of Baym's Φ in terms of the screened interaction which is shown in Fig. 4. With different weightings (as determined by a coupling-constant integration), these are also diagrams for the exchange-correlation energy E_{xc} (for Φ there is also a "Hartree" diagram which is not shown). To guarantee an approximation to be fully consistent, it must consist of the sum of one or more of these diagrams with the self-energy Σ for the fully interacting propagators G being given by $\Sigma=\delta\Phi/\delta G$. Normally, as a practical matter one usually either replaces any uniform-gas propagator by noninteracting uniform-gas propagators after any functional derivations have been done, or else supposes that this propagator modification is absorbed into some other part of an approximation scheme. We discuss in Sec. III A how we shall treat this problem in this paper.

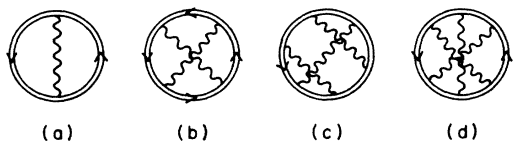

FIG. 3. Diagrams for Baym's Φ. The exchange-correlation energy may be obtained by the appropriate coupling-constant integration. The wiggly lines are defined in Fig. 4. The double solid lines are the fully interacting propagators.

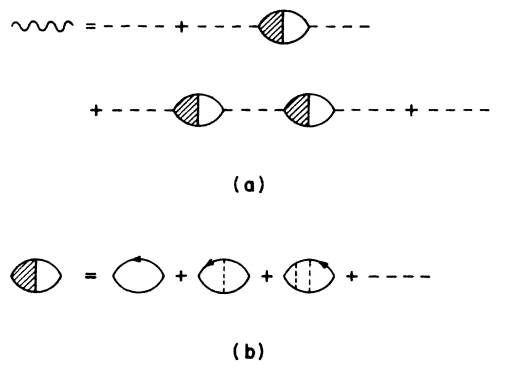

FIG. 4. (a) Wiggly line is the screened Coulomb interaction given by (A5). The dashed lines are bare Coulomb interactions. The bubbles are the density polarization parts. The shaded areas in the bubbles are irreducible vertex parts; (b) several lowest-order terms for these vertex parts.

For the uniform gas the so-called random-phase approximation consists of Fig. 3(a) alone, evaluated with noninteracting propagators, and using only the first term in Fig. 4(b) as the kernel in the series 4(a) for the screened interaction. This produces[19] the term proportional to $\ln r_s$ in (2.1), after subtracting the so-called exchange energy $E_x=-0.9163/r_s$ [the latter is simply Fig. 3(a) to lowest order in the bare interaction]. On the other hand, if $\ln(r_s)$ is considered to be of the same order as other terms of order r_s^0, then Fig. 3(b) must be included as well. The high-density limit ($r_s\to 0$) is given exactly by the sum of these two diagrams.[19] Figure 2 shows that the correction of ~ 0.04 Ry to the RPA is probably not very density dependent in comparison with the RPA itself. This in turn suggests that we adopt the approximation of Figs. 3(a) and 3(b) as our basic approximation.

However attractive a possibility this may seem, it does not satisfy the criterion (i) of simplicity. Even in the uniform system, Fig. 3(b) is a ninefold integration; it has been evaluated only at $r_s\to 0$ and this took the brute force of Gell-Mann's and Brueckner's[19] approximate Monte Carlo numerical evaluation or the brilliance of Onsager[20] to produce an analytic evaluation. Therefore further approximation had to be made.

The approximation actually made seems crude by modern standards, but it was all we could devise that allowed us to carry out the evaluation for the nonuniform system using the scheme of Ref. 9 without further approximation. What we did was to follow Hubbard[22] and replace one of the wiggly lines in Fig. 3(b) by a static interaction

$$V_c(k)\equiv 4\pi e^2/(k^2+k_F^2)\ ,$$

where k_F is the Fermi momentum and k is the momentum transfer along the other line. This is equivalent to an expansion of Hubbard's original approximation to second order in the bare potential. We also use a static potential to approximate first-order self-energy corrections [for example, in Fig. 5(b)]. Thus we use V_c to approximate first-order self-energy corrections and first-order vertex corrections [i.e., Fig. 5(c)] and neglect higher corrections. In contrast, Hubbard used V_c to include vertex corrections in a ladder approximation to all orders. We find *a posteriori* that our approximation is better than Hubbard's, apparently because of cancellation among higher-order terms [e.g., Fig. 3(c) was included approximately by Hubbard but Fig. 3(d) was not].

Making the approximation described above gives

$$\Delta E_c=\tfrac{1}{2}\int\frac{d^3k}{(2\pi)^3}\int_c\frac{d\omega}{2\pi i}\int_0^1 d\lambda\frac{1}{\lambda}g(k)V_\lambda(\mathbf{k})\times\left[\frac{1}{\epsilon_\lambda(\mathbf{k},\omega)}-1\right]\chi_{0u}(\mathbf{k},\omega)\ , \tag{2.2}$$

where the contour c encloses the positive real axis in the positive (counterclockwise) sense. The factor $g(k)$ is the Hubbard factor:

$$g(k)=-k^2/[2(k^2+k_F^2)]\ , \tag{2.3}$$

while $V_\lambda(\mathbf{k})=8\pi\lambda/k^2$, and $\epsilon_\lambda(\mathbf{k},\omega)$ is the RPA dielectric function

$$\epsilon_\lambda(\mathbf{k},\omega)=1-V_\lambda(\mathbf{k})\chi_{0u}(\mathbf{k},\omega)\ . \tag{2.4}$$

The function $\chi_{0u}(\mathbf{k},\omega)$ is the density response of the uniform system to a unit screened potential, as a function of the coupling constant λ. For the most part we retain the notation of Ref. 9, so that $\chi_{0u}(\mathbf{k},\omega)=P(\mathbf{k},\omega+i0)$ with

$$P(\mathbf{k},\omega)=P^+(\mathbf{k},\omega)+P^-(\mathbf{k},\omega)\ , \tag{2.5}$$

$$\tilde{P}(\mathbf{k},\omega)=P^+(\mathbf{k},\omega)-P^-(\mathbf{k},\omega)\ , \tag{2.6}$$

and

$$P^+(\mathbf{k},\omega)=\frac{1}{\Omega}\sum_{\mathbf{K},\sigma}\frac{f_{\mathbf{K}}}{\omega-\varepsilon_{\mathbf{K}+\mathbf{k}}+\varepsilon_{\mathbf{K}}}\ , \tag{2.7}$$

and

$$P^-(\mathbf{k},\omega)=\frac{1}{\Omega}\sum_{\mathbf{K},\sigma}\frac{-f_{\mathbf{K}+\mathbf{k}}}{\omega-\varepsilon_{\mathbf{K}+\mathbf{k}}+\varepsilon_{\mathbf{K}}}\ , \tag{2.8}$$

thus correcting a misprint in Eq. (3.7) of that paper. The quantity $\tilde{P}$ is listed here for completeness, but will not be used until later.

The expression (2.2) is readily evaluated and is plotted as the solid line in Fig. 2. Comparison with the presumably more accurate points discussed earlier shows that this approximation is really quite good. At high densities its error is somewhat less than 0.01 Ry, and this quite likely remains true over the whole range. Our calculation also lies virtually on top of the points calculated by Singwi *et al.*[14] (SSTL); the latter have almost become an accepted standard of comparison, as they have been parameterized by Hedin and Lundqvist[15] and are widely used in electronic-structure calculations. Note also that our calculation quite likely is a considerable improvement over Hubbard's original approximation, except at $r_s\to 0$, where they coincide (the value cited by Hubbard of $\Delta E_c=0.036$ Ry at $r_s=0$ is inaccurate; the correct value is $\Delta E_c=0.0415$ Ry).

In Table I we tabulate the present calculation along

TABLE I. Correlation energies (in Ry) from various theoretical calculations.

r_s	−1.0	−2.0	−3.0	−4.0	−5.0	−6.0
RPA[a]	−0.158	−0.124	−0.106	−0.094	−0.085	−0.078
Hubbard[b]	−0.131	−0.102	−0.087	−0.077	−0.069	−0.064
Present[c]	−0.126	−0.097	−0.081	−0.071	−0.064	−0.058
SSTL[d]	−0.125	−0.097	−0.080	−0.070	−0.063	−0.057
Average[e]	−0.123	−0.092	−0.076	−0.066	−0.058	−0.054
CA[f]	−0.120	−0.090			−0.056	
Freeman[g]	−0.118	−0.088	−0.073	−0.064	−0.057	−0.052

[a]Numerical calculation of the RPA.
[b]Reference 22.
[c]Equation (2.2).
[d]Reference 14.
[e]Average of Vosko *et al.*, Ref. 2.
[f]Ceperley and Adler, Ref. 21.
[g]Reference 23.

with several others for comparison. Aside from the original Hubbard approximation, another approximation similar to ours has been made by Freeman.[23] He also effectively gave an approximation to Fig. 3(b) which yields a ΔE_c slightly larger than ours, possibly because only one of the two wavy lines was screened.

III. BEYOND-RPA CORRECTIONS TO THE GRADIENT EXPANSION

A. General theory

In the preceding section we adopted a Hubbard-like approximation to obtain corrections of the second-order exchange type to the RPA. Here we use the same kind of approximation to calculate the corresponding corrections to the lowest-order coefficient in the gradient expansion. In addition, we calculate the self-energy corrections of the same order which make a contribution to the nonuniform case.

We define the desired gradient coefficient $B_{\rm xc}$ in the usual way by

$$E = E_{\rm LDA} + \int d^3x (\nabla n)^2 B_{\rm xc}(n) , \tag{3.1}$$

where E is the ground-state energy functional and $E_{\rm LDA}$ is its value in the local-density approximation (LDA), and $n = n(\mathbf{x})$ is the electronic density. As previously discussed,[6–9] the expansion (3.1) is not directly applicable to real systems, but Langreth and Mehl[6,7] (LM) devised a practical scheme where the knowledge of $B_{\rm xc}$ represented a first step. We have found it numerically intractable to carry out a wave-vector decomposition of the deviation from the RPA, as was done[9] for the RPA. Fortunately, in this case we do not expect large (spurious) contributions at small wave vector, so that it probably makes sense simply to add the correction which we will calculate to the nonlocal exchange-correlation approximation of LM.

The calculation proceeds by expanding the diagrams of Fig. 3 to second order in an external potential which produces the nonuniformity in density, and then eliminating the potential in favor of the density; the result is then expanded in powers of various deviations of the density. We follow Ma and Brueckner[16] and express the formal results of this process in terms of the exact density-response function of the uniform system $\chi(\mathbf{q},\omega)$ evaluated at $\omega=0$. The equivalent method of Langreth and Perdew[9] could also have been used, but its extra complication is unnecessary if a wave-vector analysis is not going to be performed.

In developing approximate diagrammatic expressions for $E_{\rm xc}$, and hence the coefficient $B_{\rm xc}$ in (3.1), it is important to maintain self-consistency in the sense of Baym[18] insofar as one is able. Langreth[24] has recently shown that the Kohn-Sham relation

$$\delta E_{H\rm xc} = \int d^3x\, v_{H\rm xc}(\mathbf{x}) \delta n(\mathbf{x}) \tag{3.2}$$

is valid not only for the exact theory, but for any Φ-derivable (in the sense of Baym) approximation as well. We have, for notational simplicity, added the Hartree term

$$\int n(\mathbf{x}_1) n(\mathbf{x}_2) (e^2/r_{12}) d^3x_1\, d^3x_2$$

to the exchange-correlation energy $E_{\rm xc}$ to make $E_{H\rm xc}$, and similarly have added its functional densities to the exchange-correlation potential $v_{\rm xc}(\mathbf{x})$ to form $v_{H\rm xc}(\mathbf{x})$, which is the difference between the Kohn-Sham potential $v_0(\mathbf{x})$ [which when acting on a noninteracting system gives the true density $n(\mathbf{x})$] and the true one-electron potential $v_1(\mathbf{x})$. Taking the second functional derivative and setting $v_1 = v_0 = 0$ to find the perturbation from a uniform system gives

$$\frac{\delta^2 E_{H\rm xc}}{\delta n(\mathbf{x}) \delta n(\mathbf{x}')} = -\frac{\delta v_1(\mathbf{x})}{\delta n(\mathbf{x}')} + \frac{\delta v_0(\mathbf{x}')}{\delta n(\mathbf{x}')} , \tag{3.3}$$

where we have used the fact that $v_{H\rm xc} = v_0 - v_1$. The right-hand side of (3.3) may be expressed in terms of the irreducible polarization propagator χ that is the density response to a fully screened potential. Writing $\bar{\chi} = \delta n / \delta v_1$ and $\bar{\chi}_0 = \delta n / \delta v_0$ and noting that $\bar{\chi}^{-1} = \chi^{-1} - V$, where V is the Coulomb interaction

$$V(\mathbf{x},\mathbf{x}') = e^2 / |\mathbf{x} - \mathbf{x}'| ,$$

we see that

$$\left.\frac{\delta^2 E_{\rm xc}}{\delta n(\mathbf{x})\delta n(\mathbf{x}')}\right|_{v_1=0} = -\chi^{-1}(\mathbf{x}-\mathbf{x}') + \chi_0^{-1}(\mathbf{x}-\mathbf{x}') , \tag{3.4}$$

where χ_0 is the value of χ for the noninteracting system. In writing (3.4) we have also used the fact that

$$\delta^2 E_{H\rm xc}/\delta n \delta n' = \delta^2 E_{\rm xc}/\delta n \delta n' + V$$

and $\chi_0 = \bar{\chi}_0$. Therefore the change in $E_{\rm xc}$ due to the nonuniformity is

$$\Delta E_{\rm xc} = \tfrac{1}{2}\int d^3x \int d^3x' \delta n(\mathbf{x})\delta n(\mathbf{x}') \times [-\chi^{-1}(\mathbf{x}-\mathbf{x}') + \chi_0^{-1}(\mathbf{x}-\mathbf{x}')] . \tag{3.5}$$

Upon Fourier transforming (3.1) and (3.5) and expanding,

$$\chi(q) = a + bq^2 + \cdots , \tag{3.6a}$$

$$\chi_0(q) = a_0 + b_0 q^2 + \cdots . \tag{3.6b}$$

We find by equating powers of q^2 that

$$B_{\rm xc} = \tfrac{1}{2}(ab^2 - a_0 b_0^2) . \tag{3.7}$$

The formula (3.7) first derived by Ma and Brueckner[16] for the exact theory is thus shown to follow directly from the structure of perturbation theory for any Φ-derivable approximation.

We use the above procedure to make a connection between the particular diagrams we use for $E_{\rm xc}$ (and Φ) and our approximation for $B_{\rm xc}$, although we are, of course, able to maintain Φ derivability only approximately.

The procedure for calculating $B_{\rm xc}$ should then be clear: (1) pick a closed set of diagrams from Fig. 3; (2) functionally differentiate it twice so as to obtain the corresponding approximation for χ. This establishes the correspondence between a particular closed diagram for $E_{\rm xc}$ and the corresponding diagrams for χ. Step (2) above may be accomplished in several different ways, which are equivalent. For example, one might take the closed diagrams to have the weightings appropriate to Baym's Φ, in which case the irreducible particle-hole interaction is obtained by differentiating twice with respect to the propagator G; χ is then obtained by solving the appropriate Bethe-Salpeter equation. Alternatively, one might use the self-energy obtained by $\Sigma = \delta\Phi/\delta G$ in the Dyson equation to calculate G and hence the density; χ is then obtained by a single functional differentiation with respect to the screened potential. Here we actually use a third method better suited to our approximation scheme, but which again is equivalent, and which will be discussed below.

We note that real fully interacting propagators should, in principle, be used to evaluate the solid lines in the diagram with the self-energies Σ determined by the relation $\Sigma = \delta\Phi/\delta G$. If we *define* the RPA to *mean* the evaluation of the diagram of Fig. 3(a) with noninteracting propagators, then it is clear that the RPA does not rigorously meet the Φ-derivability standard, although it was argued by Langreth and Perdew[9] that the correction obtained by using real propagators in this diagram would be largely nullified by cancellation between contributions coming from *a* and *b* respectively, in (3.7). This fact was also verified by Geldart and Rasolt.[17]

The approximate approach which we adopt here in calculating beyond-RPA contributions is to suppose that the diagrams of Fig. 3 can be categorized by the number of *screened* Coulomb lines in each part of the diagram when expanded in terms of noninteracting propagators. Thus the first three diagrams of Fig. 3 would become the diagrams of Figs. 5(a)–5(c) plus higher-order corrections [for example, Figs. 5(d)–5(f)], where here the solid line is the noninteracting propagator. The approximation of retaining only Figs. 5(a)–5(c) is Φ derivable to the extent that the diagrams containing three or more screened potential lines are small. Since we find that 5(b) and 5(c) make a fairly small correction to 5(a), at the densities we consider, we conclude that this is reasonable.

This is certainly our experience with the uniform system as well. In this case diagram 5(c) evaluated with unscreened potential lines gives the leading correction to the RPA [5(a)], while diagram 5(b) with unscreened potential lines rigorously vanishes. For the nonuniform system we find that the lines must be screened to prevent logarithmic divergences in otherwise small corrections. Furthermore, 5(b) does not vanish for the nonuniform system (even with bare potential lines) and therefore it must be kept for consiestency with 5(c). One may wonder at this point why it was unnecessary to include 5(b) in the uniform case discussed earlier, since it is necessary to use dynamically screened potential lines. The answer is that while, in general, 5(b) does not vanish, even in the uniform case, we find that it *does* in fact vanish within the Hubbard-like approximation adopted in this paper.

Since our approximation scheme is now expressed in terms of G_0, it is most convenient to use the following scheme for generating the χ implied by these diagrams: We suppose that the diagrams of Fig. 5 are weighted as Baym's W; then the derivative of W with respect to a screened potential (here we do not allow Hartree self-energy insertions) gives the density n and the second derivative gives the desired correlation function χ:

$$\chi(\mathbf{x}-\mathbf{x}') = \left.\frac{\delta^2 W}{\delta\tilde{v}(\mathbf{x})\delta\tilde{v}(\mathbf{x}')}\right|_{\tilde{v}=0} , \tag{3.8}$$

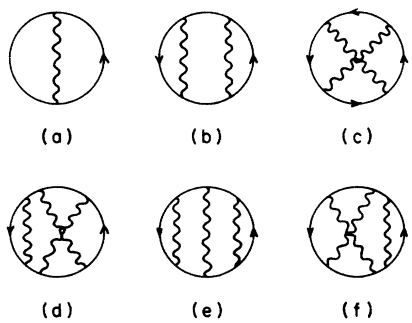

FIG. 5. Diagrams for the exchange-correlation energy in powers of wiggly lines (see text for weightings of diagrams). The solid lines are the noninteracting electron propagators. (a) RPA contribution; (b) self-energy contribution; (c) second-order exchange contribution; (d)–(f) higher-order terms.

where W contains the diagrams of Fig. 5 (no Hartree insertions) and $\tilde{v}$ is the Hartree potential that produces the nonuniformity.

B. Second-order exchange contribution

The contribution to $B_{xc}(n)$ from Fig. 5(a) has been evaluated by Langreth and Perdew[9] (LP). It will be referred to as the RPA contribution. Geldart and Rasolt[17] (GR) using (3.7) also evaluated it. Both treatments considered the effect of higher-order terms: in LP's approximation they cancelled exactly, leaving only the result in Fig. 5(a); in GR's approximation the cancellation was not exact, leaving a difference between the two treatments which became greater as density got lower. We will discuss this difference further in the next section.

We do not repeat Langreth's and Perdew's calculation of the RPA contribution. Instead, we take their result and add it to the contribution from Figs. 5(b) and 5(c) which are evaluated here and in the next subsection (III C). We only list the expressions for the RPA contribution in Appendix C for reference.

We consider Fig. 5(c) in this subsection. Following the procedure outlined in the preceding subsection, we take functional derivatives of W twice with respect to $\tilde{v}(\mathbf{q})$, the Hartree potential which causes the nonuniformity of the system. The resulting diagrams are shown in Fig. 6. One can see that they are part of $\chi(\mathbf{q},0)$. We can proceed to expand Fig. 6 in powers of q. The zeroth- and second-order terms are the contributions to a and b, respectively, according to (3.6). We label them a_{2x} and b_{2x}. They are needed in evaluating $B_{xc}(n)$.

The calculation of Fig. 6 is quite involved, especially in the presence of the dynamically screened Coulomb lines, and we make the Hubbard-like approximation we used in the uniform case. We address our approximation first, then outline the calculational procedure.

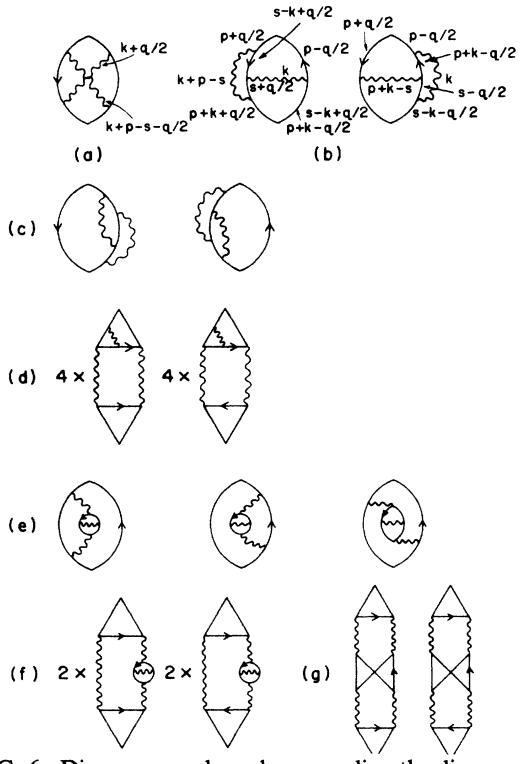

FIG. 6. Diagrams produces by expanding the diagram in Fig. 5(c) to second power in the external potential $\tilde{v}(\mathbf{q})$, which causes the nonuniformity of the system. The solid lines are noninteracting electron propagators and the wiggly lines are defined in Fig. 4.

1. *The Hubbard-like approximation*

The prescription for this approximation is straightforward: we replace one of the Coulomb lines by the static potential

$$V_c(\mathbf{k})=4\pi e^2/(k^2+k_F^2)\ ,$$

where $\mathbf{k}$ is the momentum along the other Coulomb line. However, the situation here is more complicated. In some of the diagrams in Fig. 6, not all the Coulomb lines are equivalent in their effect. For example, the ones in the bubbles of Fig. 6(f) are less critical than those connecting the triangles. We can view the diagrams in Fig. 6(f) as two triangles connected by two Coulomb lines with different screening. Replacing the wiggly lines in the bubbles by V_c simply produces a minor change on the screening of one of these lines, while replacing those wiggly lines outside of the bubbles drastically changes the screening from dynamic to static. Obviously we should choose the first way if we wish to minimize the damage caused by making the Hubbard-like approximation. For the same reason, in Fig. 6(e) we choose to replace the wiggly lines in the small bubbles, which again can be regarded as parts of the screening of the Coulomb lines attached to the big bubbles. As a result, their screening is modified but remains frequency dependent. For Fig. 6(d) we replace the wiggly lines in the triangles. From the experience of Langreth and Perdew, the wiggly lines connecting the triangles have a great impact on the result and hence should be kept intact if possible. On the other hand, each of the Coulomb lines inside the triangles may be replaced by a static V_c without causing serious error. We now summarize the way we apply the Hubbard-like approximations. For Figs. 6(a) and 6(c), it makes no difference which wiggly line is replaced. Hence we choose to replace

$$V(\mathbf{k}+\mathbf{p}-\mathbf{s})/\epsilon(\mathbf{k}+\mathbf{p}-\mathbf{s},\omega+p_0-s_0)\ ,$$

where $(\mathbf{p},p_0)$, $(\mathbf{k},\omega)$, and $(\mathbf{s},s_0)$ form four-momenta. For Fig. 6(b) we do this in a symmetric way, i.e., we replace the line on the side of the bubble in the first diagram and the crossing wiggly line in the second diagram (or vice versa). In Fig. 6(d) the lines in the triangles, and in Figs. 6(e) and 6(f) the ones in the small bubbles, are replaced by $V_c(\mathbf{k})$. Finally, complexity forced us to neglect the diagrams of Fig. 6(g). Fortunately, they are less important at high densities than the others. This can be seen by expanding in powers of e^2. The contribution from Fig. 6(g) is proportional to e^6, while that of Figs. 6(a)—6(c) are of the order of $e^4\ln e^2$ and those of Figs. 6(d)—6(f) are of the order of e^4. This means that at least at the higher densities these terms should be negligible. A more complete

discussion is given in Appendix A.

We can reduce the error in making the Hubbard-like approximation even further. The diagrams in Fig. 6 are to be expanded in powers of q. In many terms we have to expand the screened Coulomb interaction, which later will be replaced by the potential we proposed before. An expanded

$$v(k+p-s)=\frac{V(\mathbf{k}+\mathbf{p}-\mathbf{s}+\mathbf{q})}{\epsilon(\mathbf{k}+\mathbf{p}-\mathbf{s}+\mathbf{q},\omega+p_0-s_0)}$$

in powers of q can be quite different from an expanded $V_c(\mathbf{k}+\mathbf{q})$. The inaccuracy can be much greater than that in the uniform case, where V_c need not be expanded. Hence we try to avoid taking derivatives of $V_c(\mathbf{k})$. In Figs. 6(a)–6(c) there are terms with either

$$[\mathbf{q}\cdot\nabla v(k+p-s)]^2$$

or

$$v(k+p-s)(\mathbf{q}\cdot\nabla)^2 v(k+p-s)\ .$$

The former can be converted to the latter by integration by parts. For the latter we can choose to replace the $v(k+p-s)$, which is not acted upon by gradient operators by $V_c(\mathbf{k})$. In Figs. 6(d)–6(f) we can always change variables such that the Coulomb interactions to be replaced by V_c do not depend on $\mathbf{q}$, and hence need not be expanded. As a result we can completely avoid expanding V_c.

2. Analytical results

We are now ready to evaluate. Firstly, the finite-temperature–diagram technique is used to write the expressions for Fig. 6. Then the expressions are expanded in powers of q. Finally, the Hubbard-like approximation is applied with the choice of the replacement mentioned before. Some details are in Appendix A. Here we simply show the result. The zeroth-order term in q is a_{2x} and the second-order term is $b_{2x}q^2$:

$$a_{2x}=\frac{a_0^2}{\Omega}\sum_{\mathbf{k}} g(k)\int_c \frac{d\omega}{2\pi i}V(\mathbf{k})\left[B_0(\mathbf{k},\omega)\left[\frac{1}{\epsilon(\mathbf{k},\omega)}-1\right][U+1]+2\Lambda_0^2(\mathbf{k},\omega)v(k)[2U^2+4U+1]\right]+c_0 a_0^2\ , \tag{3.9}$$

$$\begin{aligned} b_{2x}q^2=\frac{1}{\Omega}\sum_{\mathbf{k}} g(\mathbf{k})\int_c \frac{d\omega}{2\pi i}V(\mathbf{k})\Bigg[&B_2(\mathbf{k},\mathbf{q},\omega)\left[\frac{1}{\epsilon(\mathbf{k},\omega)}-1\right][U+1] \\ &+4\Lambda_0(\mathbf{k},\omega)\left[\Lambda_2(\mathbf{k},\mathbf{q},\omega)-\frac{(\mathbf{q}\cdot\nabla)^2}{8}\Lambda_0(\mathbf{k},\omega)\right]v(k)[2U^2+4U+1] \\ &+\Lambda_0^2(\mathbf{k},\omega)\left[\frac{(\mathbf{q}\cdot\nabla)^2}{2}v(k)\right][U^2+2U+1]+\Lambda_0^2(\mathbf{k},\omega)v(k)\frac{(\mathbf{q}\cdot\nabla)^2}{2}[U^2+2U] \\ &-\Lambda_0^2(\mathbf{k},\omega)[\mathbf{q}\cdot\nabla v(k)]\mathbf{q}\cdot\nabla[U^2+2U]\Bigg]+c_2\ , \end{aligned} \tag{3.10}$$

where

$$v(k)=\frac{V(\mathbf{k})}{\epsilon(\mathbf{k},\omega)}\ , \tag{3.11}$$

$$U=\frac{1}{\epsilon(\mathbf{k},\omega)}-1 \tag{3.12}$$

$$\Lambda_0(\mathbf{k},\omega)=-\frac{1}{2}\frac{\partial P(\mathbf{k},\omega)}{\partial\mu}\ , \tag{3.13a}$$

$$\begin{aligned}\Lambda_2(\mathbf{k},\mathbf{q},\omega)=&-\frac{(\mathbf{q}\cdot\nabla)^2}{12}\frac{\partial P(\mathbf{k},\omega)}{\partial\mu}-\frac{q^2}{6}\frac{\partial^2\tilde{P}(\mathbf{k},\omega)}{\partial\mu\partial\omega} \\ &+\frac{q^2}{6}\frac{\partial^2 P(\mathbf{k},\omega)}{\partial\omega^2}+\frac{q^2}{12}\frac{\partial^2 P(\mathbf{k},\omega)}{\partial\mu^2}\ , \end{aligned} \tag{3.13b}$$

$$B_0(\mathbf{k},\omega)=\frac{1}{2}\frac{\partial^2 P(\mathbf{k},\omega)}{\partial\mu^2}\ , \tag{3.14a}$$

$$\begin{aligned}B_2(\mathbf{kq},\omega)=\frac{1}{12}\Bigg[&\frac{(\mathbf{q}\cdot\nabla)^2}{2}\frac{\partial^2 P(\mathbf{k},\omega)}{\partial\mu^2}+q^2\frac{\partial^3\tilde{P}(\mathbf{k},\omega)}{\partial\mu^2\partial\omega} \\ &-q^2\frac{\partial^3 P(\mathbf{k},\omega)}{\partial\mu^3}-q^2\frac{\partial^3 P(\mathbf{k},\omega)}{\partial\omega^2\partial\mu}\Bigg]\ . \end{aligned} \tag{3.14b}$$

The contour c encloses the positive real axis in the counterclockwise sense. The Hubbard factor $g(k)$ is defined in (2.3). The quantities c_0 and c_2 are that LP called chemical-potential-shift terms. Following the procedure of Sec. III [LP (Ref. 9)], we get

$$c_0=-\frac{1}{2k_F^2}\frac{\partial(\Delta E_c)}{\partial\mu}\ , \tag{3.15}$$

$$c_2=-\frac{q^2}{24k_F^4}\frac{\partial(\Delta E_c)}{\partial\mu}\ , \tag{3.16}$$

where ΔE_c was defined in (2.2). $\partial(\Delta E_c)/\partial\mu$ can be obtained by breaking any electron line in each beyond-RPA closed diagram [in our case, Fig. 5(c)]. Again using the finite-temperature–diagram technique and applying the Hubbard-like approximation, we find

$$\begin{aligned}\frac{\partial(\Delta E_c)}{\partial\mu}=-\frac{2}{\Omega}\sum_{\mathbf{k}}\int_c\frac{d\omega}{2\pi i}g(k)V(\mathbf{k})\Lambda_0(\mathbf{k},\omega) \\ \times\left[\frac{1}{\epsilon(\mathbf{k},\omega)}+\frac{\ln[\epsilon(\mathbf{k},\omega)]}{1-\epsilon(\mathbf{k},\omega)}\right]\ . \end{aligned} \tag{3.17}$$

In (3.9) and (3.10), the terms with B's were called the Hartree-Fock–type terms and the ones with Λ's were called fluctuation terms by Langreth and Perdew.[9] The diagrams in Figs. 6(a)–6(c) contribute to both, those in 6(d) and 6(f) contribute to the latter, and those in Fig. 6(e) contribute to only the former. To be more specific, we can identify the contribution of each set of diagrams by looking at the quantity in the last pair of small square brackets of each term in (3.9) and (3.10). The terms with zeroth power of U are from Figs. 6(a)–6(c) and those with second power are from Fig. 6(f). Figure 6(d) contributes to terms with the first power of U in the fluctuation part and Fig. 6(e) contributes to those with first power in the Hartree-Fock–type part.

3. *Numerical evaluation*

Equations (3.9)–(3.17) are readily evaluated numerically. To do so, we average over the angle of $\mathbf{q}$ and make following variable changes:

$$k \to x = \tfrac{1}{2}k/k_F \,, \tag{3.18a}$$

$$\omega \to y = -\tfrac{1}{4}i\omega/k_F^2 \,. \tag{3.18b}$$

We then deform the contour c to the real axis on y plane. As a result (3.9) and (3.10) become, respectively,

$$a_{2x} = -\frac{e^2 a_0^2}{2(2\pi)^4}\int_0^\infty dx \int_0^\infty dy\, z_0(x,y) \,, \tag{3.19}$$

$$b_{2x} = -\frac{e^2}{2(2\pi)^4 4k_F^2}\int_0^\infty dx \int_0^\infty dy\, z_2(x,y) \,, \tag{3.20}$$

where

$$z_0(x,y) = z_{0h} + z_{0f} + z_{0c} \,, \tag{3.21}$$

$$z_2(x,y) = z_{2h} + z_{2f} + z_{2c} \,. \tag{3.22}$$

Subscripts h, f, and c denote the Hartree-Fock–type part, the fluctuation part, and the chemical-potential-shift part, respectively. The z's on the right-hand sides of (3.21) and (3.22) are defined in Appendix B. They are related to $B_0(\mathbf{k},\omega)$, $B_2(\mathbf{k},\mathbf{q},\omega)$, $\Lambda_0(\mathbf{k},\omega)$, $\Lambda_2(\mathbf{k},\mathbf{q},\omega)$, and $\partial\Delta E_c/\partial\mu$ with variable changes in (3.18).

We note that in the process of deforming contour c and changing variables, a discontinuity at the origin of the ω plane has to be taken care of. It is due to the fact that poles move in or out of the contour along the real axis as $|\mathbf{k}|$ increases from less than $2k_F$ to greater. This leads to a singular term at $k = 2k_F$ or $x = 1$, whose contribution to b_{2x} is

$$\frac{e^2}{4k_F^2(2\pi)^3}\int_0^\infty dk\, g(k)\left[\tfrac{11}{9}\delta(k-2k_F)\left(\frac{1}{\epsilon^2(k,0)}-\frac{1}{\epsilon(k,0)}\right)+\tfrac{1}{9}\delta'(k-2k_F)\left(\frac{1}{\epsilon^2(k,0)}-\frac{1}{\epsilon(k,0)}\right)\right.$$
$$\left.+\frac{s^2}{6}\delta(k-2k_F)\left(\frac{2}{\epsilon^3(k,0)}-\frac{1}{\epsilon(k,0)}\right)\right] \,, \tag{3.23}$$

where

$$s^2 = \tfrac{1}{4}k_{\mathrm{FT}}^2/k_F^2 = e^2/2\pi k_F \tag{3.24}$$

and k_{FT} is the Fermi-Thomas wave vector. The form of (3.23) is somewhat similar to the RPA version given by Langreth and Perdew,[9] although the contribution here comes from the diagrams of Fig. 6. The most singular terms are now only δ functions because our expressions have been integrated by parts; higher-order distributions would have appeared if we were to insist (as LP did) that k corresponded to the wave vector of the structure factor or of $E_{\mathrm{xc}}(k)$ as defined in Ref. 9.

We are now ready to put all the pieces together. The expressions of z's in Appendix B are substituted into (3.21) and (3.22), which are, in turn, inserted into (3.19) and (3.20). a_{2x} and b_{2x} are evaluated by performing x and y integrations numerically. Finally, (3.23) should be added to the integrated value of b_{2x}. We will present the results of our calculation in Sec. IV.

C. Self-energy contribution in second order

We evaluate the contribution associated with Fig. 5(b) in this subsection. It was accounted for previously by Geldart and Rasolt[17] and by Langreth and Perdew.[9] Geldart and Rasolt divided it into two parts: the vertex part and the higher-order self-energy part. The former was obtained by taking functional derivatives of the wiggly lines or the solid-line sections which begin and end with the same wiggly line. In other words, it came from taking derivatives of a self-energy part. The latter was from the solid lines without self-energy. The vertex part was approximated by a constant factor $[1/(1-\eta)$ in their notation] and was cancelled by the "compressibility enhancement" from the constant a in (3.6a). The higher-order self-energy part was argued to give a similar factor and incorporated implicitly. Langreth and Perdew treated the contribution of Fig. 5(b) as a whole. Similarly, they approximated it as a constant factor which cancelled the compressibility enhancement. The difference between these two approaches lies in the treatment of the higher-order self-energy terms. This leads to different results at low densities. We are going to calculate both the vertex part and the higher-order self-energy part, and examine their cancellation with the compressibility enhancement from a explictly.

To get a clearer picture, we expand a and b in (3.6a) in powers of the wiggly line,

$$a = a_0 - (a_{\mathrm{RPA}} + a_{2x} + a_2 - a_{\mathrm{RPA}}^2/a_0) + \cdots \,, \tag{3.25}$$

$$b = b_0 + b_{\mathrm{RPA}} + b_{2x} + b_2 + \cdots \,, \tag{3.26}$$

where a_0 and b_0 were defined in (3.6b), a_{RPA} and b_{RPA} are the RPA terms from Fig. 5(a), a_{2x} and b_{2x} are the

second-order contributions [Fig. 5(c)] which we evaluated in Sec. III B, and a_2 and b_2 are the self-energy contributions from Fig. 5(b). We substitute (3.25) and (3.26) into (3.7) and get

$$B_{xc}(n)=\frac{a_0^2}{2}(b_{RPA}-2b_0a_{RPA}/a_0+b_{2x} -2b_0a_{2x}/a_0+b_2-2b_0a_2/a_0 -2b_{RPA}a_{RPA}/a_0+3b_0a_{RPA}^2/a_0^2) . \quad (3.27)$$

$B_{xc}(n)$ in (3.27) included all the terms up to the second order of the wiggly line. Thus we expect $B_{xc}(c)$ to be quite accurate in the high- and even in the intermediate-density range. The sum of the first two terms in (3.27) was evaluated by LP. The next two were calculated in Sec. III B. Now we concentrate on the rest. Later we will see that there is a cancellation between them, though it is not complete. The uncancelled part is calculated by the Hubbard-like approximation.

To evaluate a_2 and b_2, we first take functional derivatives of Fig. 5(b) twice, as we did in (3.8). The resulting diagrams are shown in Fig. 7. We then expand the expressions for them in powers of q. The zeroth- and second-order terms give a_2 and b_2, respectively. These diagrams are quite complicated. We calculated them indirectly by taking advantage of the existing RPA expressions. Consider first the RPA-like diagrams of Fig. 8. They are RPA diagrams with free-electron propagators replaced by interacting ones with the self-energy shown in Fig. 9(a). If we expand them in powers of the self-energy, the zeroth-order ones are the RPA diagrams and the first-order ones are almost the same as those in Fig. 7. The difference between Fig. 7 and them is shown in Fig. 10. Thus, instead of evaluating the diagrams in Fig. 7, we work on Figs. 8 and 10. The former, though they look complicated, can be evaluated by a quasi-RPA expression, while the latter will be calculated explicitly.

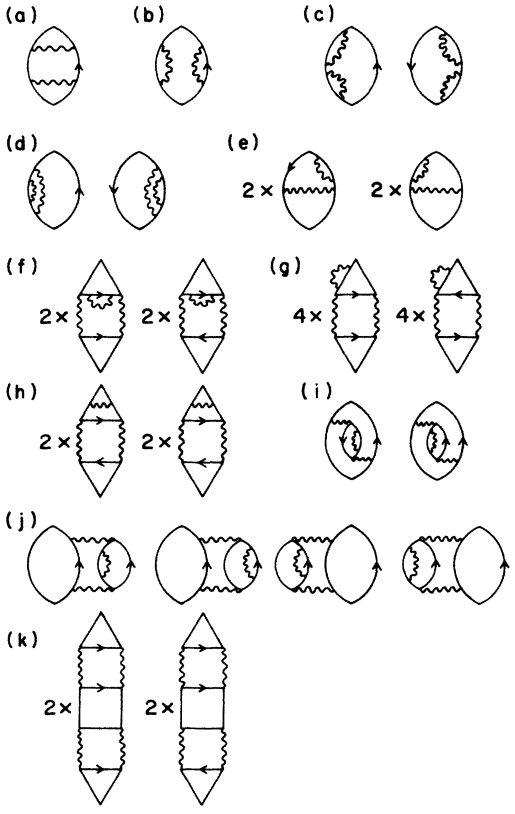

FIG. 7. Diagrams produced by expanding the diagram in Fig. 5(b) to second power in an external potential $\tilde{v}(\mathbf{q})$. Solid lines and wiggly lines are the same as those in Fig. 6.

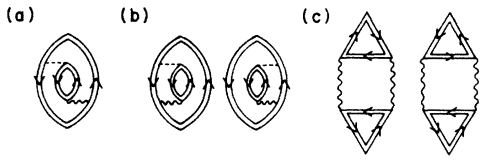

FIG. 8. RPA-like diagrams. They arise from expanding the RPA diagram in Fig. 5(a) to second order in $\tilde{v}(q)$, then replacing every noninteracting electron propagator by a double solid line. The latter is an interacting electron line with the self-energy in Fig. 9(a).

1. The RPA-like diagrams

We make a further approximation to calculate Fig. 8. The self-energy of each double line in Fig. 8 is approximated by Fig. 9(b) with the dotted line having the form $V_c(\mathbf{k})$. This approximation is consistent with our previous Hubbard-like approximation in the sense that we always replace screened Coulomb lines by the same form. As a result, the self-energy can be calculated analytically:

$$\Sigma(\mathbf{p})=-\frac{e^2}{\pi}\left\{k_F+\frac{2k_F^2-p^2}{4p}\ln\left|\frac{(p+k_F)^2+k_F^2}{(p-k_F)^2+k_F^2}\right| -k_F\left[\tan^{-1}\left(\frac{q+k_F}{k_F}\right) -\tan^{-1}\left(\frac{p-k_F}{k_F}\right)\right]\right\} . \quad (3.28)$$

Note that $\Sigma(\mathbf{p})$ is frequency independent. This enables us to perform the frequency summation as if the self-energy were not present when we calculate Fig. 8.

With the above approximation and existing RPA expressions (in Appendix C), we can write the expressions for Fig. 8 immediately. The major difference from the RPA expressions is that now we have interacting propagators. Thus, instead of $P(\mathbf{k},\omega)$ and $\tilde{P}(\mathbf{k},\omega)$, which are

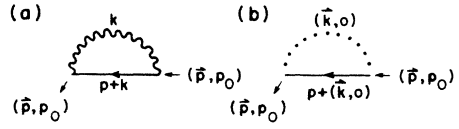

FIG. 9. (a) Self-energy $\Sigma(\mathbf{p},p_0)$; (b) an approximate form of $\Sigma(\mathbf{p},p_0)$. The dotted line is a statically screened Coulomb line $4\pi e^2/(k^2+k_F^2)$.

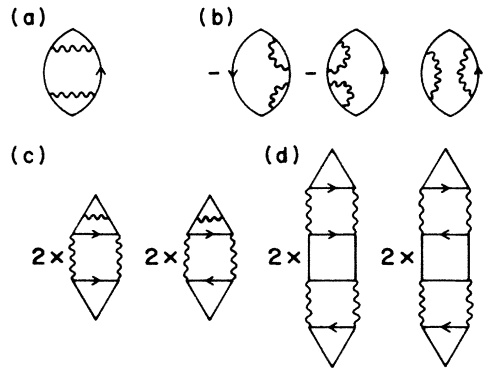

FIG. 10. Difference between Fig. 7 and the first-order terms (in powers of the self-energy) of the diagrams in Fig. 8.

relevant in the RPA expressions, we have $P'(\mathbf{k},\omega)$ and $\tilde{P}'(\mathbf{k},\omega)$, which contain the self-energy parts:

$$P'(\mathbf{k},\omega)=\frac{1}{\Omega}\sum_{\mathbf{k},\sigma}\frac{f_{\mathbf{p}}-f_{\mathbf{p}+\mathbf{k}}}{\omega-\varepsilon_{\mathbf{p}+\mathbf{k}}-\Sigma(\mathbf{p}+\mathbf{k})+\varepsilon_{\mathbf{p}}+\Sigma(\mathbf{p})}\ , \tag{3.29a}$$

$$\tilde{P}'(\mathbf{k},\omega)=\frac{1}{\Omega}\sum_{\mathbf{k},\sigma}\frac{f_{\mathbf{p}+\mathbf{k}}+f_{\mathbf{p}}}{\omega-\varepsilon_{\mathbf{p}+\mathbf{k}}-\Sigma(\mathbf{p}+\mathbf{k})+\varepsilon_{\mathbf{p}}+\Sigma(\mathbf{p})}\ , \tag{3.29b}$$

where σ is the spin index and

$$f_{\mathbf{p}}=\begin{cases}1 \text{ if } \varepsilon_{\mathbf{p}}+\Sigma(\mathbf{p})<\mu\ ,\\ 0 \text{ if } \varepsilon_{\mathbf{p}}+\Sigma(\mathbf{p})>\mu\ .\end{cases} \tag{3.30}$$

The expressions for Fig. 8 are the same as those of the RPA with minor modification of definitions of $\Lambda_0(\mathbf{k},\omega)$, $\Lambda_2(\mathbf{k},\mathbf{q},\omega)$, $B_0(\mathbf{k},\omega)$, $B_2(\mathbf{k},\mathbf{q},\omega)$, and $v(k)$. They are presented also in Appendix C. This relation is simple because the RPA diagrams and those in Fig. 8 are very similar.

We now work out the contribution from the self-energy. This combined with the known RPA result gives us the contribution from Fig. 8 to a_2 and b_2. As a first step, we simplify $P'(k,\omega)$ and $\tilde{P}'(k,\omega)$. Langreth and Perdew pointed out that in the RPA expressions the small-$|\mathbf{k}|$ part dominates. This is also true for Fig. 8 since the additional quantity $\Sigma(\mathbf{p})$ is a smooth function and hence cannot change the small-$|\mathbf{k}|$ behavior very much. Therefore our simplified $P'(\mathbf{k},\omega)$ and $\tilde{P}'(\mathbf{k}',\omega)$ should perserve their original small-k behavior.

We expand $\Sigma(\mathbf{p}+\mathbf{k})$ in powers of k:

$$\Sigma(\mathbf{p}+\mathbf{k})=\Sigma(\mathbf{p})+\varepsilon_{\mathbf{p}+\mathbf{k}}-\varepsilon_{\mathbf{p}})\frac{1}{2p}\frac{\partial\Sigma(\mathbf{p})}{\partial p}+\cdots$$
$$\approx\Sigma(\mathbf{p})+(\varepsilon_{\mathbf{p}+\mathbf{k}}-\varepsilon_{\mathbf{p}})\left[\frac{1}{2p}\frac{\partial\Sigma(\mathbf{p})}{\partial p}\right]\Bigg|_{p=k_F}\ . \tag{3.31}$$

The second line follows because $(1/2p)[\partial\Sigma(\mathbf{p})/\partial p]$ varies slowly as a function of $|\mathbf{p}|$. We substitute (3.31) into Eqs. (3.30) to obtain approximations for $P'(\mathbf{k},\omega)$ and $\tilde{P}'(\mathbf{k},\omega)$,

$$P'(\mathbf{k},\omega)\approx\frac{1}{\Omega}\sum_{\mathbf{k},\sigma}\frac{f_{\mathbf{p}}-f_{\mathbf{p}+\mathbf{k}}}{\omega-d(\varepsilon_{\mathbf{p}+\mathbf{k}}-\varepsilon_{\mathbf{p}})}=\frac{P(\mathbf{k},\omega/d)}{d}\ , \tag{3.32a}$$

$$\tilde{P}'(\mathbf{k},\omega)\approx\frac{1}{\Omega}\sum_{\mathbf{k},\sigma}\frac{f_{\mathbf{p}}+f_{\mathbf{p}+\mathbf{k}}}{\omega-d(\varepsilon_{\mathbf{p}+\mathbf{k}}-\varepsilon_{\mathbf{p}})}=\frac{\tilde{P}(\mathbf{k},\omega/d)}{d}\ , \tag{3.32b}$$

where

$$d=1+\left[\frac{1}{2p}\frac{\partial\Sigma(\mathbf{p})}{\partial p}\right]\Bigg|_{p=k_F}\ . \tag{3.33}$$

Thus we have kept the small-$|\mathbf{k}|$ behavior of $P'(\mathbf{k},\omega)$ and $\tilde{P}'(\mathbf{k},\omega)$ very well. The same thing can be said about the expressions for Fig. 8 in which the most important functions are $P'(\mathbf{k},\omega)$, $\tilde{P}'(\mathbf{k},\omega)$, and their derivatives.

The quantities $f_{\mathbf{p}}$ and $f_{\mathbf{p}+\mathbf{k}}$ in Eqs. (3.32) are those defined in (3.30). When we take derivatives of $P'(\mathbf{k},\omega)$ and $\tilde{P}'(\mathbf{k},\omega)$ with respect to μ, the chemical potential (μ derivatives do not act on d, see Appendix C), a factor of d^{-1} appears since

$$\frac{\partial f_{\mathbf{p}}}{\partial\mu}=-\frac{\delta(|\mathbf{p}|-2k_F)}{d}\ .$$

The derivative with respect to ω also results in the factor $1/d$ because on the right-hand sides of Eqs. (3.32) we have ω/d instead of ω.

We substitute Eqs. (3.32) into (C5)–(C10), change ω to ω/d in the integral, and take into account the factors produced by the μ and ω derivatives to find that the contribution of Fig. 8 is just $1/d$ times that of the RPA with e^2 replaced by e^2/d. The evaluation of the contribution of Fig. 8 to a_2 and b_2 is therefore trivial.

2. *Diagrams in Fig. 10*

We now turn our attention to Fig. 10. The diagrams of Fig. 10(d) were too complicated to be reasonably evaluated. Fortunately, they are higher order in r_s (actually they are of order r_s^3) and our experience with terms of this order is that they are very small for $r_s<6$, so that our neglect of them is not serious. Figure 10(a) can be evaluated analytically if the statically screened potential $V_c(\mathbf{k})$ is used. We denote it by $\chi_v(\mathbf{q})$. Using Feyman rules, one finds

$$\chi_v(\mathbf{q})=2\int\frac{d^3k}{(2\pi)^3}\int\frac{d^3k'}{(2\pi)^3}\int\frac{d^3k''}{(2\pi)^3}\frac{4\pi e^2}{(\mathbf{k}-\mathbf{k}')^2+k_F^2}\frac{4\pi e^2}{(\mathbf{k}-\mathbf{k}'')^2+k_F^2}\frac{f_{\mathbf{q}+\mathbf{k}'}-f_{\mathbf{q}}}{\varepsilon_{\mathbf{q}+\mathbf{k}'}-\varepsilon_{\mathbf{q}}}\frac{f_{\mathbf{q}+\mathbf{k}}-f_{\mathbf{q}}}{\varepsilon_{\mathbf{q}+\mathbf{k}}-\varepsilon_{\mathbf{q}}}\frac{f_{\mathbf{q}+\mathbf{k}''}-f_{\mathbf{q}}}{\varepsilon_{\mathbf{q}+\mathbf{k}''}-\varepsilon_{\mathbf{q}}}\ . \tag{3.34}$$

$\chi_v(q)$ is expanded in powers of q to give its contributions to a_2 and b_2, which are denoted as a_{2v} and b_{2v}:

$$a_{2v}=-0.6476s^4(k_F/2\pi^2)^{-1}\,, \tag{3.35}$$

$$b_{2v}=0.098\,86s^4/2\pi^2k_F\,. \tag{3.36}$$

The diagrams in Fig. 10(b) are simply the second-order terms in powers of wiggly lines of the diagram in Fig. 11, where the double lines are the interacting electron propagators with the self-energy Σ in Fig. 9(a). Again the approximate Σ in Fig. 9(b) is used and we find the form of Fig. 11 to be

$$\sum_{\mathbf{p},\sigma}\frac{f_{\mathbf{p}+\mathbf{q}}-f_{\mathbf{p}}}{\varepsilon_{\mathbf{p}}+\Sigma(\mathbf{p})-\varepsilon_{\mathbf{p}+\mathbf{q}}-\Sigma(\mathbf{p}+\mathbf{q})}\,.$$

We use the approximate form of $\Sigma(\mathbf{p}+\mathbf{q})$ in (3.31), retain only the second-order terms in e^2 and q, and obtain a_{2e} and b_{2e}, which are contributions of Fig. 10(b) to a_2 and b_2:

$$a_{2e}=-0.042\,882s^4(k_F/2\pi^2)^{-1}\,, \tag{3.37}$$

$$b_{2e}=0.042\,882s^4/24\pi^2k_F\,. \tag{3.38}$$

We evaluate Fig. 10(c) by making a Hubbard-like approximation such that the wiggly lines in triangles become static interactions $V_c(\mathbf{k})$. This is again consistent with the approximations we made before. As a result, the diagrams in Fig. 10(c) become those in Fig. 12. The contribution to the term $-2b_0a_2/a_0$ in (3.27) is at least of the order $e^6(r_s^3)$ and can be neglected for our purposes. The contribution to b_2 has two parts: the part in which the prefactor is expanded in powers of q and the part where the diagrams in the parentheses are expanded. The former is again discarded because it is of order e^6. The latter just consists of some RPA diagrams (those in parentheses) times the factor

$$\frac{2}{a_0}\left[-\frac{1}{2}\right]\frac{4\pi e^2}{k^2+k_F^2}\bigg|_{k=k_F}=2a_1/a_0\,, \tag{3.39}$$

where a_1 is the first-order term of a in e^2. Note that a_{RPA} consists of a_1 and higher-order terms in e^2. For the next-to-last term in (3.27), we approximate a_{RPA} by a_1 because the higher-order terms are very small compared to a_1 in the physically interesting density region. Thus

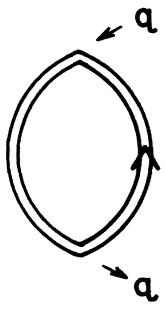

FIG. 11. Part of the density response function $\chi(\mathbf{q},0)$. The double line is the interacting electron line with the self-energy of Fig. 9(b).

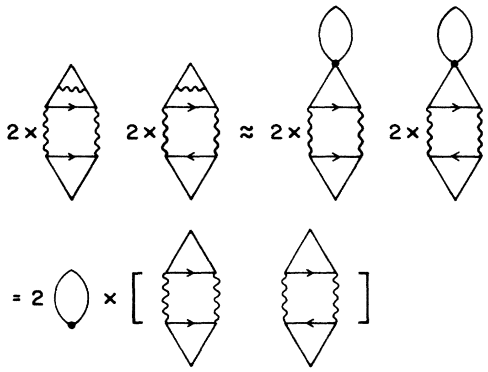

FIG. 12. Here the diagrams in Fig. 10(c) are simplified by the Hubbard-like approximation described in the text.

Fig. 12 cancels part of the next-to-last term in (3.27). The remaining contribution is shown in Fig. 13. Having applied the Hubbard-like approximation to the wiggly lines, we find its contribution to $B_{\mathrm{xc}}(n)$, which is the sum of Fig. 10(c) and the next-to-last term in (3.27), is $-2(a_1/a_0)b_{2d}$, where

$$b_{2d}=0.080\,95s^2/2\pi^2k_F\,. \tag{3.40}$$

3. Summary

We have now all the pieces of a_2 and b_2. The last term in (3.27) is evaluated with the knowledge of following quantities:

$$a_0=-(k_F/2\pi^2)^{-1}\,, \tag{3.41}$$

$$b_0=+1/24\pi^2k_F\,, \tag{3.42}$$

$$a_{\mathrm{RPA}}\approx-0.6s^2(2\pi^2/k_F)\,, \tag{3.43}$$

where a_{RPA} is evaluated using the static potential $V_c(\mathbf{k})$. We feel that since there is strong cancellation between various terms in (3.27), as suggested by Geldar, Rasolt, Langreth, Perdew, and the present workers, it is better to use the same potential for all the terms involved.

Now we have evaluated all the terms in (3.27). We use the result of Langreth and Perdew for the first two (RPA) terms. They, along with the fifth, sixth, and seventh term in (3.27), give the following contributions: (i) The RPA diagrams with self-energy insertions (Fig. 8), which give a result which is $1/d$ times the RPA result with s^2 replaced by s^2/d; (ii) the sum of the diagrams in Fig. 10 and the term $-2a_{\mathrm{RPA}}b_{\mathrm{RPA}}/a_0$ in (3.27); these give

$$a_0^2[b_{2v}+b_{2e}-2b_0(a_{2v}+a_{2e})/a_0-2b_{2d}a_1/a_0]/2\,.$$

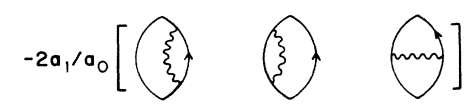

FIG. 13. A factor $-2a_1/a_0$ times the difference between the RPA diagrams and those in Fig. 12.

The quantities a_{2x} and b_{2x} have been evaluated in Sec. III B. The modification due to the self-energy insertion is the same as in the RPA case. We put the quantities a_{2x} and b_{2x} with self-energy insertions on the right-hand side of (3.27) (these are $1/d$ times the a_{2x} and b_{2x} evaluated in Sec. III B, respectively, with e^2 replaced by e^2/d). Finally, the last term in (3.27) can be evaluated with (3.41)—(3.43). The resulting $B_{xc}(n)$ is given in Sec. IV.

IV. RESULTS

The results of the calculations of the preceding two sections are collected here. As in previous papers, they are given in terms of the dimensionless quantity Z defined by writing the coefficient B_{xc} appearing in the gradient expansion as

$$B_{xc}=[e^2\pi/16(3\pi^2 n)^{4/3}]Z \ . \tag{4.1}$$

If we let Z_{RPA} be the value calculated by LP, then our results can be summarized in a gross sense by the approximate *fit* (see Fig. 14)

$$Z-Z_{RPA}=-0.08r_s \ , \tag{4.2}$$

for $r_s<6$. The above is *not* a series expansion of our results and there are logarithmic corrections at small r_s (these go as $r_s \ln r_s$), but (4.2) should be useful (and adequate) for any numerical use of our results. Our actual calculated Z is shown in Fig. 15, along with the RPA results of LP and the results of GR. The latter were called RPA by GR, but included an approximation to some of the terms which in the terminology here are beyond RPA. The closeness of our present results to the calculation of GR indicates that their approximation scheme was quite good; however, since the terms not included by them are individually often quite large, there was no obvious way to have determined this *a priori*.

V. DEVIATIONS FROM THE RPA AS A SELF-INTERACTION "ERROR"

It is well known within the local-density approximation (LDA) that when one calculates energy differences involving the removal of one or more electrons, one finds a non-negligible difference between the RPA result (as implemented, for example, via the von Barth—Hedin formula[25]) and the results obtained from a scheme regarded as more accurate [for example, the Hedin-Lundqvist fit of the SSTL (Ref. 13) calculation or one of the[2,10] fits to the Ceperly-Alder sampling]. This difference generally turns out to be around 0.04 Ry per electron. The source of this difference is for the most part the fact that the more accurate theories contain all terms to second order in e^2 while the RPA does not. At high densities the contributing non-RPA term for the uniform case (LDA) is the second-order exchange term whose value is 0.048 Ry per electron.[19,20] For an extended nonuniform system the second-order self-energy corrections are no longer cancelled by the chemical-potential shift and therefore contribute as well. We will argue here that, at least for contributions arising from localized orbitals isolated in real space, this type of correction is a spurious self-interaction error, which one can most simply correct by using the RPA (e.g., von Barth—Hedin) in the LDA expression rather than the "better" approximations.

One hint of the nature of this correction is evident from the work of Cole and Perdew,[13] who found that when the self-interaction error was subtracted out via the method of Perdew and Zunger,[10] there was little difference between the results obtained in RPA and those obtained in "better" approximations.

The more important observation, however, is that at least at high densities the main correction to the RPA arises from those terms in second-order perturbation theory not included in the RPA. This fact was noticed Gell-Mann and Brueckner[19] and exploited by Nozières and Pines.[26] The second-order terms in question are exchangelike and in diagrammatic terms [see Figs. 5(b) and 5(c)] consist of but a single-electron closed loop. This

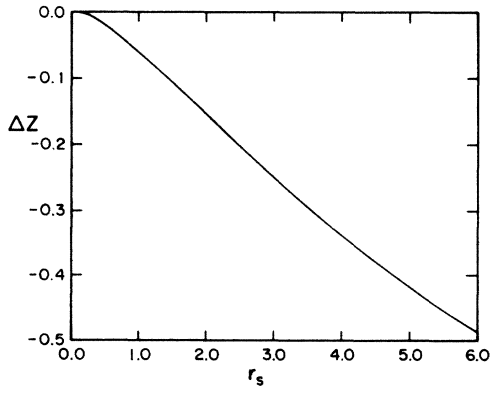

FIG. 14. The difference between the Z from present calculation and that from the RPA of LP, Ref. 9. It can be fitted by a straight line with slope -0.08.

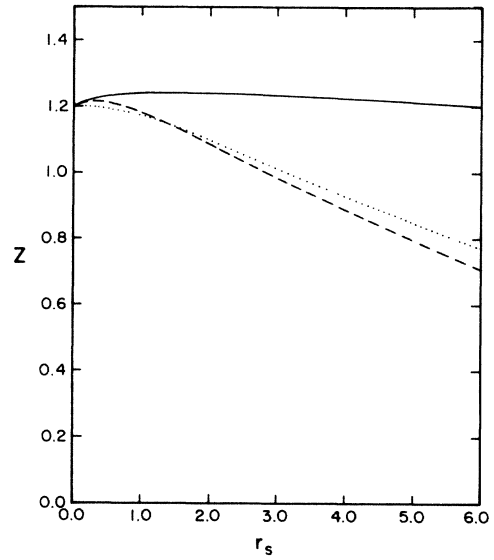

FIG. 15. Z vs r_s, where $Z=[16/(\pi e^2)]k_F^4 B(n)$. The solid line is from the RPA calculation by Langreth and Perdew (Ref. 9). The dashed line is the present result and the dotted line is that of Geldart and Rasolt.

means that to the extent which the relevant localized electron orbitals occupy separate regions of real space, this correction is zero. It is exactly zero for the neutral helium atom. It is not zero for the LDA to the helium atom. This means, of course, that one should not make this sort of correction to the RPA version of the LDA unless one also includes the corresponding nonlocal correction which will tend to cancel it.

Let us now see to what extent the nonlocal correction just obtained [Eq. (4.2)] *does* cancel most of the beyond-RPA local correction of ~ 0.04 Ry/electron. We estimate this by calculating this correction for a pair of electrons of opposite spins in a single exponential orbital, giving a number density of

$$n(r)=(4\pi J^3)^{-1}\exp(-r/J) . \tag{5.1}$$

If (4.2) indeed represents a term which will cancel an error of ~ 0.03 Ry/electron, then it should be independent of the orbital size J. Substitution of (4.1) and (4.2) into (3.1) gives

$$[e^2\pi/16(3\pi^2)^{4/3}]\int_0^\infty dr\, 4\pi r^2[(\nabla n)^2/n^{4/3}](-0.08r_s) . \tag{5.2}$$

Using (5.1) for n in (5.2) (with $\frac{4}{3}\pi r_s^3=n^{-1}$) gives -0.06 Ry, independent of J, as expected. Since this is for two electrons, the correction per electron is -0.03 Ry, which is just about right to cancel the correction of $+0.04$ Ry which comes from the correction to the RPA in the LDA.

The choice then arises as to what one should do in actual calculations on real systems, in cases where corrections to the local-density approximation are needed. The first possibility would be to use the "best" uniform E_{xc} in the local-density approximation (probably one of the fits[2,10] to the Ceperly-Alder points,[21] or the Hedin-Lundqvist formula, which for the nonpolarized case is almost the same); to this one would add the nonlocal correction which comes from the Langreth-Mehl[6,7] scheme, and finally add the correction from (4.2), as given by (5.2). The second method would simply be to use the RPA version of the LDA (e.g., von Barth–Hedin[25]) plus the Langreth-Mehl[6,7] nonlocal correction. In so doing we anticipate that the cancellation exhibited above will occur.

Of the two methods, we strongly lean toward the latter. The main reason for this follows. First, in deriving (4.2) we have been unable to make a wave-vector analysis; although the correction under consideration is not expected to have the large spurious long-range part like the RPA gradient expansion,[9] nevertheless, in some situations a long-wavelength cutoff as introduced in Refs. 6 and 7 is surely going to be important; in the absence of a wave-vector analysis this cannot be implemented. Secondly, the correction (4.2) increases in magnitude with lowering density—that is just where our confidence in the approximations used to derive (4.2) begin to fail. On the other hand, our arguments leading to the cancellation are quite general and should hold for densities rapidly varying enough for nonlocal effects to be important at all.

In conclusion then, we believe that Eq. (5.1) of LM, Ref. 7, still represents the best nonlocal correction we have to offer. It has now been tested for valence and core states of atoms, molecules,[27] bulk solids,[28] and surfaces[29] with excellent results.

ACKNOWLEDGMENT

This work was supported in part by the National Science Foundation under Grant No. NSF-DMR-83-04210.

APPENDIX A

Here we expand the diagrams in Fig. 6 in powers of e^2 to see their contribution to b in the high-density limit. We also show some details of the calculation mentioned in Sec. III B. We deal with Figs. 6(a)–6(c) first. It is straightforward to use the finite-temperature-diagram technique to write expressions for them:

$$\begin{aligned}2\int dk\int dp\int ds\{&v(k+q/2)v(k+p-s-q/2)[G(p+q/2)G(p-q/2)G(p+k)G(s-k)G(s-q/2)G(s+q/2)]\\&+v(k-q/2)v(k+p-s)[G(p+q/2)G(p-q/2)G(p+k)G(s-k-q/2)G(s-k+q/2)G(s)]\\&+v(k)v(k+p-s-q/2)[G(p+q/2)G(p-q/2)G(p+k+q/2)G(p+k-q/2)G(s)G(s-k)]\\&+v(k)v(k+p-s)[G(p)G(p+q)+G(p+k)G(p+k+q)]G(p)G(p+k)G(s)G(s-k)\} ,\end{aligned} \tag{A1}$$

where k,p,s are four-momenta, $G(p)$ is a free-electron Green's function, and

$$\int dp=\int\frac{d^3p}{(2\pi)^3}\sum_{p_0}\frac{1}{2\pi i} , \tag{A2}$$

$$v(k)=V(\mathbf{k})/\epsilon(\mathbf{k},\omega) . \tag{A3}$$

We note that the first term in the curly braces of (A1) is from Fig. 6(a), the middle two are from Fig. 6(b), and the last one is from Fig. 6(c). By setting q in (A1) to zero, we get the contribution to a. For b, we expand (A1) to second order in q. Using the following identities,

$$G(p)(\mathbf{q}\cdot\nabla)^2G(p)=(\mathbf{q}\cdot\nabla)^2G^2(p)/3+2q^2G^3(p)/3 , \tag{A4}$$

$$G^2(p)(\mathbf{q}\cdot\nabla)^2G(p)=(\mathbf{q}\cdot\nabla)^2G^3(p)/6+q^2G^4(p)\ , \tag{A5}$$

integrating by parts, and changing variables, we get

$$\begin{aligned}\tfrac{1}{2}\int ds\int dp\int dk\{&\tfrac{1}{2}[G^2(p)G(p+k)+G(p)G^2(p+k)][G^2(s)G(s-k)+G(s)G^2(s-k)]v(k+p-s)(\mathbf{q}\cdot\nabla)^2v(k)\\&-G^2(p)G(p+k)G^2(s)G(s-k)\mathbf{q}\cdot\nabla v(k)\mathbf{q}\cdot\nabla v(k+p-s)\\&+\tfrac{1}{12}[G(p)(\mathbf{q}\cdot\nabla)^2G^2(p+k)+8q^2G(p)G^3(p+k)+G(p+k)(\mathbf{q}\cdot\nabla)^2G^2(p)+8q^2G(p+k)G^3(p)]\\&\times[G^2(s)G(s-k)+G(s)G^2(s-k)]v(k)v(k+p-s)\\&+\tfrac{1}{6}[G^2(p)(\mathbf{q}\cdot\nabla)^2G^2(p+k)+8q^2G^2(p)G^3(p+k)+G^2(p+k)(\mathbf{q}\cdot\nabla)^2G^2(p)+8q^2G^2(p+k)G^3(p)]\\&\times G(s)G(s-k)v(k)v(k+p-s)+\tfrac{1}{6}G(s)G(s-k)v(k)v(k+p-s)\\&\times[2G(p+k)(q\cdot\nabla)^2G^3(p)+12q^2G(p+k)G^4(p)+2G(p)(\mathbf{q}\cdot\nabla)^2G^3(p+k)+12q^2G(p)G^4(p+k)]\}\ .\end{aligned} \tag{A6}$$

We note that without screening, that is, using V's instead of v's in (A6), there would be divergence at small $|\mathbf{k}|$. This is due to the long-range behavior of the Coulomb interaction. It can be seen easily. Using the bare Coulomb potential, we can perform the summations over frequencies. The first term in (A6) becomes

$$\tfrac{1}{4}\int\frac{d^3p}{(2\pi)^3}\int\frac{d^3s}{(2\pi)^3}\int\frac{d^3k}{(2\pi)^3}\frac{(f'_{\mathbf{p}+\mathbf{k}}-f'_{\mathbf{p}})(f'_{\mathbf{s}}-f'_{\mathbf{s}-\mathbf{k}})}{2\mathbf{k}\cdot(\mathbf{k}+\mathbf{p}-\mathbf{s})}\times V(\mathbf{k}+\mathbf{p}-\mathbf{s})(\mathbf{q}\cdot\nabla)^2V(\mathbf{k})\ , \tag{A7}$$

where $f'_{\mathbf{p}}=\partial f_{\mathbf{p}}/\partial\mu$. For small $|\mathbf{k}|$, $f'_{\mathbf{p}+\mathbf{k}}-f'_{\mathbf{p}}$ and $f'_{\mathbf{s}}-f'_{\mathbf{s}-\mathbf{k}}$ are proportional to k. Thus the integrand is proportional to k^{-3}. This leads to an infrared logarithmic divergence after integration. Similar behavior is found for some other terms in (A6).

With screening, we are not able to perform the frequency summations analytically. However, we can apply our Hubbard-like approximation to (A6), i.e., substitute $V_c(\mathbf{k})$ for $v(k+p-s)$. This will not change the order of (A6) in e^2 in the high-density limit since there is no divergence at $|\mathbf{k}+\mathbf{p}-\mathbf{s}|=0$. Thus, we can sum over s_0 and p_0. This first term in (A6) becomes

$$\int dk\int\frac{d^3p}{(2\pi)^3}\int\frac{d^3s}{(2\pi)^3}\frac{f'_{\mathbf{p}+\mathbf{k}}-f'_{\mathbf{p}}}{\omega-\varepsilon_{\mathbf{p}+\mathbf{k}}+\varepsilon_{\mathbf{p}}}\frac{f'_{\mathbf{s}}-f'_{\mathbf{s}-\mathbf{k}}}{\omega-\varepsilon_{\mathbf{s}}+\varepsilon_{\mathbf{s}-\mathbf{k}}}\times V_c(\mathbf{k})(\mathbf{q}\cdot\nabla)^2v(k)\ . \tag{A8}$$

We change the ω summation into an integration by standard methods and replace ω by y, where

$$y=-\tfrac{1}{2}i\omega/k_Fk\ . \tag{A9}$$

For small $|\mathbf{k}|$, the dielectric function has the form

$$\epsilon(\mathbf{k},\omega)\approx1+\frac{2e^2k_F}{\pi k^2}\left[1-y\tan^{-1}\left[\frac{1}{y}\right]\right]\ . \tag{A10}$$

Thus $(\mathbf{q}\cdot\nabla)^2v(\mathbf{k})$ has the approximate form

$$(\mathbf{q}\cdot\nabla)^2v(\mathbf{k})=\frac{4\pi e^2(-2q^2)}{\{k^2+(2e^2k_F/\pi)[1-y\tan^{-1}(1/y)]\}^2}+\cdots\ . \tag{A11}$$

We substitute (A9) and (A11) into (A8) and expand (A8) in powers of e^2. The $\mathbf{k}$ integration is easily performed. The result shows that the leading term of (A8) is proportional to $e^4\ln e^2$. The other terms of (A6) are of the same order. Therefore Figs. 6(a)—6(b) contribute to b a term proportional to $e^4\ln e^2$ in the high-density limit.

The orders of other diagrams in Fig. 6 are easy to ascertain if they are compared with the RPA diagrams. The diagrams in Figs. 6(d)—6(f) are an order higher in wiggly lines than the RPA terms. Therefore, they are of the order e^4 since the latter is proportional to e^2 in the high-density limit. The one in Fig. 6(g) are of the order e^6 since they are two orders higher in wiggly lines.

To evaluate a_{2x} we set q to zero in (A1) and then apply the Hubbard-like approximation. For b_{2x} we apply the approximation to (A6). After very lengthy algebra, we reach (3.9) and (3.10).

APPENDIX B

Here we show the expression for the z's in (3.19) and (3.20):

$$z_{0h}=gh_0(1/\epsilon-1)/\epsilon\ , \tag{B1}$$

$$z_{0f}=(s^2/x^2)gf_0^2(2/\epsilon^2-1)/\epsilon\ , \tag{B2}$$

$$z_{0c}=z_{2c}=2gf_0[1/\epsilon+\ln\epsilon/(1-\epsilon)]\ , \tag{B3}$$

$$z_{2h}=gh_2(1/\epsilon-1)/\epsilon\ , \tag{B4}$$

$$\begin{aligned}z_{2f}=s^2g\Bigg[&4f_0f_2\left[\frac{2}{\epsilon^2}-1\right]\\&+f_0^2\left[\frac{2}{x^2}+\frac{2\epsilon_x}{x\epsilon}-\frac{\epsilon_{xx}}{\epsilon}+\frac{2\epsilon_x^2}{\epsilon^2}\right]\Big/6\epsilon^2\\&+f_0^2\left[-\frac{2\epsilon_x}{x\epsilon}+\frac{3\epsilon_x^2}{\epsilon^2}-\frac{\epsilon_{xx}}{\epsilon}\right]\Big/3\epsilon^2\\&-f_0^2\left[\frac{2}{x}+\frac{\epsilon_x}{\epsilon}\right]\frac{2\epsilon_x}{3\epsilon^2}\Bigg]\Big/x^2\epsilon\ ,\end{aligned} \tag{B5}$$

where

$$s^2=\tfrac{1}{4}k_{\rm FT}^2/k_F^2=e^2/2\pi k_F\ , \tag{B6}$$

where $k_{\rm FT}$ is the Fermi-Thomas wave vector, and g,ϵ are the same functions as $g(k)$ and $\epsilon(\mathbf{k},\omega)$ with variable changes in Eqs. (3.18):

$$g=-\frac{1}{2}\frac{x^2}{x^2+\frac{1}{4}}\ , \tag{B7}$$

$$\epsilon=1+(s^2/x^2)(\tfrac{1}{2}+x^2F)\ , \tag{B8}$$

and

$$x^2F=-\frac{y^2+x^2(1-x^2)}{8x^3}\ln\left|\frac{X}{Y}\right|-\frac{y}{2x}F_2\ , \tag{B9}$$

with

$$F_2=\tan^{-1}\left|\frac{(1-x)x}{y}\right|+\tan^{-1}\left|\frac{(1+x)x}{y}\right|\ , \tag{B10}$$

$$X=y^2+x^2(1-x)^2\ , \tag{B11}$$

$$Y=y^2+x^2(1+x)^2\ . \tag{B12a}$$

Also,

$$\epsilon_x=\frac{d\epsilon}{dx}=s^2\left|G-5\frac{F}{x}-\frac{1}{x^3}\right|\ , \tag{B12b}$$

$$\epsilon_{xx}=\frac{d\epsilon_x}{dx}=s^2\left|\frac{3}{x^4}+H-10\frac{G}{x}+30\frac{F}{x^2}\right|\ , \tag{B13}$$

where

$$G=-\frac{1}{4x^4}\left|4yF_2+(1-2x^2)\ln\left|\frac{X}{Y}\right|-2x\right|\ , \tag{B14}$$

$$H=\frac{G}{x}-\frac{1}{2x^3}\left|\frac{3}{x}-2\ln\left|\frac{X}{Y}+\frac{(1-x)(1-2x)^2}{X}-\frac{(1+x)(1+2x)^2}{Y}\right|\right|\ . \tag{B15}$$

The f's and h's are related to Λ's and B's in the following way:

$$h_0=(512\pi^2k_F^3)B_0(\mathbf{k},\omega)=16\left|\frac{x(1-x)}{X}-\frac{x(1+x)}{Y}\right|\ , \tag{B16}$$

$$h_2=\int(2048\pi^2k_F^5/q^2)B_2(\mathbf{k},\mathbf{q},\omega)d\Omega_q/4\pi$$
$$=\frac{16}{9}\left|\frac{3x(1-x)}{X}-\frac{3x(1+x)}{Y}+\frac{(1+12x^2)(X-2y^2)}{4xX^2}-\frac{(1+12x^2)(Y-2y^2)}{4xY^2}+\frac{x(1-2x)^2(1-x)(X-4y^2)}{2X^3}-\frac{x(1+2x)^2(1+x)(Y-4y^2)}{2Y^3}\right|\ , \tag{B17}$$

$$f_0=(32\pi^2k_F)\Lambda_0(\mathbf{k},\omega)=-\frac{1}{x}\ln\left|\frac{X}{Y}\right|\ , \tag{B18}$$

$$f_2=\int(128\pi^2k_F^3/q^2)[\Lambda_2(\mathbf{k},\mathbf{q},\omega)-\tfrac{1}{8}(\mathbf{q}\cdot\nabla)^2\Lambda_0(\mathbf{k},\omega)]d\Omega_q/4\pi$$
$$=-\frac{1}{9x}\left|-\frac{(1-x)(6x^2-5x+3)}{X}+\frac{(1+x)(6x^2+5x+3)}{Y}-\frac{(1-2x)^2(X-2y^2)}{X^2}+\frac{(1+2x)^2(Y-2y^2)}{Y^2}+\frac{3}{2x^2}\ln\left|\frac{X}{Y}\right|\right|$$
$$-\frac{1}{12x}\left|-\frac{6x^2+6x-1}{X}+\frac{6x^2+6x+1}{Y}-\frac{2x^2(1-x)^2(1-2x)^2}{X^2}-\frac{2x^2(1+x)^2(1+2x)^2}{Y^2}\right|\ . \tag{B19}$$

APPENDIX C

Here we show the RPA expressions and those for Fig. 8. For the RPA

$$a_{\rm RPA}=\frac{a_0^2}{\Omega}\sum_{\mathbf{k}}\left|\int_c\frac{d\omega}{2\pi i}[B_0(\mathbf{k},\omega)v(k)+2\Lambda_0^2(\mathbf{k},\omega)v^2(k)]-\frac{V(\mathbf{k})}{8\pi^2k_F}\right|-\frac{a_0^2}{2k_F^2}c_{\rm RPA}\ , \tag{C1}$$

$$b_{\rm RPA}q^2=\frac{1}{\Omega}\sum_{\mathbf{k}}\left\{\int_c\frac{d\omega}{2\pi i}\left|B_2(\mathbf{k},\mathbf{q},\omega)v(k)+4\Lambda_0(\mathbf{k},\omega)\left|\Lambda_2(\mathbf{k},\mathbf{q},\omega)-\frac{(\mathbf{q}\cdot\nabla)^2}{8}\Lambda_0(\mathbf{k},\omega)\right|v^2(k)+\Lambda_0^2(\mathbf{k},\omega)v(k)\frac{\mathbf{q}\cdot\nabla)^2}{2}v(k)-\frac{\Lambda_0^2(\mathbf{k},\omega)}{2}[\mathbf{q}\cdot\nabla v(k)]^2\right|-\frac{q^2V(\mathbf{k})}{96\pi^2k_F^2}\right|-\frac{q^2c_{\rm RPA}}{24k_F^2}\ , \tag{C2}$$

where the contour c has the same meaning as in the text, and $c_{\rm RPA}$ is the chemical-potential shift of the RPA correlation energy

$$c_{\rm RPA}=\frac{\partial E_{\rm RPA}}{\partial\mu}=-\frac{1}{\Omega}\sum_{k}\int_{c}\frac{d\omega}{2\pi i}\Lambda_0(\mathbf{k},\omega)v(k)\ . \tag{C3}$$

Equations (C1), (C2), and (C3) are derived directly from (3.6) and (3.7). Hence, their forms are different from those in Langreth and Perdew.[9] The latter, in order to carry out a wave-vector analysis, started with the expression for the exchange-correlation energy and took functional derivatives with respect to density. However, the expressions here give the same $B_{\rm xc}(n)$ as those in Ref. 9, as they must.

For Fig. 8 the expressions are very similar to (C1) and (C2). However, in the presence of the self energy in Fig. 9(b), interacting propagators, instead of the free propagators in RPA, should be used. We denote the interacting propagator with four-momentum p by $G'(p)$. The derivation of the expressions for Fig. 8 involves mostly expanding propagators in powers of q. We make a few reasonable approximations so that the expressions for Fig. 8 are almost the same as (C1) and (C2), except for a few constant factors. The approximation of the self-energy has been described in text. Here we introduce another involving expanding the interacting propagator in powers of q:

$$\begin{aligned}G'(p+q)=&G'(p)+\mathbf{q}\cdot\nabla G'(p)\\&+\tfrac{1}{2}\{\mathbf{q}\cdot\nabla[\varepsilon_{\mathbf{p}}+\Sigma(\mathbf{p})]\}^2\frac{\partial^2}{\partial\mu^2}G'(p)\\&-\tfrac{1}{2}\{(\mathbf{q}\cdot\nabla)^2[\varepsilon_{\mathbf{p}}+\Sigma(\mathbf{p})]\}\frac{\partial}{\partial\mu}G'(p)\ .\end{aligned} \tag{C4}$$

Note that the μ derivatives should not act on $\Sigma(\mathbf{p})$ in $G'(p)$ although it is a function of k_F. The factor $(\mathbf{q}\cdot\nabla)^2[\varepsilon_{\mathbf{p}}+\Sigma(\mathbf{p})]$ of the last term of (C4) is approximated by $2q^2d$, where d is defined in (3.33). This is in the same spirit with the approximations in (3.31)–(3.33). With this simplification, the contributions of Fig. 8 to a and b have exactly the same forms of (C1) and (C2), respectively, except that $B_0(\mathbf{k},\omega)$, $B_2(\mathbf{k},\mathbf{q},\omega)$, $\Lambda_0(\mathbf{k},\omega)$, $\Lambda_2(\mathbf{k},\mathbf{q},\omega)$, and $v(k)$ are replaced by $B_0'(\mathbf{k},\omega)$, $B_2'(\mathbf{k},\mathbf{q},\omega)$, $\Lambda_0'(\mathbf{k},\omega)$, $\Lambda_2'(\mathbf{k},\mathbf{q},\omega)$, and $v'(k)$. We list their definitions here:

$$B_0'(\mathbf{k},\omega)=\frac{1}{2}\frac{\partial^2}{\partial\mu^2}P'(\mathbf{k},\omega)\ , \tag{C5}$$

$$B_2'(\mathbf{k},\mathbf{q},\omega)=\frac{1}{12}\left[\frac{(\mathbf{q}\cdot\nabla)^2}{2}\frac{\partial^2}{\partial\mu^2}P'(\mathbf{k},\omega)+q^2d\frac{\partial^3\tilde{P}'(\mathbf{k},\omega)}{\partial\mu^2\partial\omega}-q^2d\frac{\partial^3P'(\mathbf{k},\omega)}{\partial\mu^3}-q^2d\frac{\partial^3P'(\mathbf{k},\omega)}{\partial\omega^2\partial\mu}\right]\ , \tag{C6}$$

$$\Lambda_0'(\mathbf{k},\omega)=-\frac{1}{2}\frac{\partial}{\partial\mu}P'(\mathbf{k},\omega)\ , \tag{C7}$$

$$\Lambda_2'(\mathbf{k},\mathbf{q},\omega)=-\frac{(\mathbf{q}\cdot\nabla)^2}{12}\frac{\partial}{\partial\mu}P'(k,\omega)-\frac{q^2d}{6}\left[\frac{\partial^2\tilde{P}'(\mathbf{k},\omega)}{\partial\mu\partial\omega}-\frac{1}{2}\frac{\partial^2P'(\mathbf{k},\omega)}{\partial\mu^2}-\frac{\partial^2P'(\mathbf{k},\omega)}{\partial\omega^2}\right]\ , \tag{C8}$$

$$v'(k)=V(\mathbf{k})/\epsilon'(\mathbf{k},\omega)\ , \tag{C9}$$

where

$$\epsilon'(\mathbf{k},\omega)=1-v(\mathbf{k})P'(\mathbf{k},\omega+i0^+)\ . \tag{C10}$$

We compare Eqs. (C5)–(C10) with Eqs. (3.13), (3.14), (3.11), and (2.4). It is clear, for Fig. 8, that $P'(\mathbf{k},\omega)$ and $\tilde{P}'(\mathbf{k},\omega)$ have taken the respective places of $P(k,\omega)$ and $\tilde{P}(k,\omega)$ in the RPA case. There are also places where d appears in the expressions of Fig. 8. Except for these two points, there is no difference between the expressions for the RPA and Fig. 8. By using Eqs. (3.32) and taking account of the factors of d produced by the μ derivatives and the ω integration, it is straightforward to see that the respective contributions of Fig. 8 to a and b are just $1/d$ times those of the RPA with e^2 replaced by e^2/d.

*Present address: Department of Physics, Queen's University, Kingston, Ontario, Canada K7L 3N6.

[1]W. Kohn and L. J. Sham, Phys. Rev. **140**, A1133 (1965).
[2]S. H. Vosko, L. Wilk, and M. Nusair, Can. J. Phys. **58**, 1200 (1980).
[3]E. P. Wigner, Trans. Faraday Soc. **34**, 678 (1938).
[4]D. Pines and P. Nozières, *The Theory of Quantum Liquids* (Benjamin, New York, 1966), Vol. 1.
[5]U. von Barth, in *Many-Body Phenomena at Surfaces*, edited by D. C. Langreth and H. Suhl (Academic, Orlando, 1984).
[6]D. C. Langreth and M. J. Mehl, Phys. Rev. Lett. **47**, 446 (1981).
[7]D. C. Langreth and M. J. Mehl, Phys. Rev. B **28**, 1809 (1983).
[8]D. C. Langreth, in *Many-Body Phenomena at Surfaces*, Ref. 5.
[9]D. C. Langreth and J. P. Perdew, Phys. Rev. B **21**, 5469 (1980).
[10]J. P. Perdew, Chem. Phys. Lett. **64**, 127 (1979); A. Zunger, J. P. Perdew, and G. L. Oliver, Solid State Commun. **34**, 933 (1980); J. P. Perdew and A. Zunger, Phys. Rev. B **23**, 5048 (1981).
[11]M. R. Norman and D. D. Koelling, Phys. Rev. B **30**, 5530 (1984).
[12]J. D. Talman and W. F. Shadwick, Phys. Rev. A **14**, 36

(1976); J. Aashamar, T. M. Luke, and J. D. Talman, At. Data Nucl. Data Tables **22**, 443 (1978); Phys. Rev. A **19**, 6 (1979).
[13]L. A. Cole and J. P. Perdew, Phys. Rev. A **25**, 1265 (1982).
[14]K. S. Singwi, A. Sjolander, M. P. Tosi, and R. H. Land, Phys. Rev. B **1**, 1044 (1970).
[15]L. Hedin and B. I. Lundqvist, J. Phys. C **4**, 2064 (1971).
[16]S.-k. Ma and K. A. Brueckner, Phys. Rev **165**, 18 (1965).
[17]M. Rasolt and D. J. W. Geldart, Phys. Rev. Lett. **35**, 1234 (1975); D. J. W. Geldart and M. Rasolt, Phys. Rev. B **13**, 1477 (1976).
[18]G. Baym, Phys. Rev. **127**, 1391 (1962). Baym's Φ and W are weighted-diagram sums whose relationship is equivalent to the linked-cluster expansion, and such that their functional differentiations yield propagators, self-energies, etc., while maintaining all the conservation laws. See Sec. III A.
[19]M. Gell-Mann and K. A. Brueckner, Phys. Rev. **106**, 362 (1957).
[20]L. Onsagar, L. Mittag, and M. J. Stephen, Ann. Phys. (Leipzig) **18**, 71 (1966).
[21]D. M. Ceperley and B. J. Alder, Phys. Rev. Lett. **45**, 566 (1980).
[22]J. Hubbard, Proc. R. Soc. London, Ser. A **243**, 336 (1957).
[23]D. L. Freeman, Phys. Rev. B **15**, 5512 (1977).
[24]D. C. Langreth, Phys. Rev. Lett. **52**, 2317 (1984).
[25]U. von Barth and L. Hedin, J. Phys. C **5**, 1629 (1972).
[26]P. Nozières and D. Pines, Phys. Rev. **111**, 442 (1958).
[27]A. Savin, U. Wedig, H. Preuss, and H. Stoll, Phys. Rev. Lett. **53**, 2087 (1984).
[28]U. von Barth and R. Car (unpublished).
[29]A.-P. E. Mohamed and V. Sahni, Phys. Rev. B **31**, 4789 (1985).